

## Performance Evaluation of an FRP-Reinforced Concrete Bridge

Danielle K. Stone  
Ph.D. Candidate in Civil Engineering,  
University of Missouri – Rolla, Center for Infrastructure Engineering Studies,  
219 Engineering Research Lab, Rolla, MO 65409  
phone: (573) 341-6699, fax: (573) 341-6215, email: [stone@umr.edu](mailto:stone@umr.edu)

Andrea Prota,  
M.S. Candidate in Civil Engineering,  
University of Missouri-Rolla, Center for Infrastructure Engineering Studies,  
219 Engineering Research Lab, Rolla, MO 65409  
phone: (573) 341-6699, fax: (573) 341-6215, email: [prota@umr.edu](mailto:prota@umr.edu)

Antonio Nanni,  
Jones Professor of Civil Engineering,  
University of Missouri-Rolla, Center for Infrastructure Engineering Studies,  
224 Engineering Research Lab, Rolla, MO 65409  
phone: (573) 341-4553, fax: (573) 341-6215, email: [nanni@umr.edu](mailto:nanni@umr.edu)

### ABSTRACT

As part of a larger project to investigate the use of Fiber-Reinforced Polymer (FRP) materials in bridge construction, a short-span FRP-reinforced concrete bridge was installed in central Missouri. The Walters Street Bridge is a precast concrete panel bridge reinforced with both glass FRP (GFRP) and carbon FRP (CFRP) reinforcing bars. It was designed according to the American Concrete Institute's document "Guide for the Design and Construction of Concrete Reinforced with FRP Bars" to meet the load and deflection requirements of the American Association of State Highway and Transportation Officials. Carbon FRP, as tensile reinforcement, and glass FRP, as shear reinforcement, were utilized. The installation of the bridge is outlined and the results of material testing conducted on the reinforcing bars and concrete are summarized. An in-situ bridge load test was conducted, with a comparison made between the design and experimental values of maximum deflection and a discussion of the load transfer between panels is presented. Testing to determine the flexural and shear capacity of the panels was also conducted on an identical FRP-reinforced bridge panel in the laboratory; results in terms of a load-deflection diagram, ultimate load, and the failure mode of the beam are noted herein. The outcomes of these laboratory tests are further compared to the testing results of a steel-reinforced panel with the same ultimate capacity that was tested in an identical fashion.

## INTRODUCTION

The use of FRP materials in bridge construction has been increasing steadily over the last several years with the construction of bridges using FRP bridge panels, FRP bridge deck panels supported by steel stringers, and FRP bars as reinforcement for concrete. This demonstration project utilizes all three of these technologies with the overall scope including the procurement of the design, manufacturing, and installation of four bridges. A review of the installation and testing conducted on the first three bridges that utilize FRP bridge panels can be referenced in Stone et al. (1). The bridge described in this paper consists of concrete panels reinforced with FRP bars and illustrates the potential for new bridge construction. The reinforced concrete panels were pre-manufactured, transported to the site, and assembled on-site. Thus, time of construction is diminished from weeks to days with substantial benefits in terms of traffic disruption and safety.

The Walters Street Bridge consists of nine precast concrete panels, each with a depth of 0.30 m (1 ft) and a width of 0.86 m (2.83 ft). Overall, the bridge measures 7.32 m (24 ft) in span and 7.77 m (25.5 ft) in width and has a skew of approximately 12 degrees. This paper focuses on the installation of the bridge as well as testing that was conducted in the laboratory on individual panels and in-situ on the constructed bridge. In order to compare the behavior of FRP-reinforced concrete (FRP-RC) to that of steel-reinforced concrete (steel-RC), testing was conducted on two bridge panels. Comparisons will be drawn between the theoretical and experimental flexural and shear behavior of the FRP-RC panel and the steel-RC panel and the design and experimental deflections of the constructed bridge.

## DESIGN OF THE FRP-RC AND STEEL-RC PANELS

### FRP-RC Design

Utilizing the American Concrete Institute (ACI) document entitled "Guide for the Design and Construction of Concrete Reinforced with FRP Bars," (2) the bridge was designed to meet the load and deflection requirements of the American Association of State Highway and Transportation Officials (AASHTO). The bridge was designed to carry a standard HS15-44 truck loading within the span length divided by 800 deflection requirement. Strength reduction factors,  $\phi$ , of 0.7 and 0.85 were used for the flexure and shear design, respectively.

The FRP-RC panel reinforcement consists of commercially available CFRP and GFRP reinforcing bars with the following properties. For the CFRP bars, a guaranteed design tensile strength of 1862 MPa (270 ksi) and a tensile elastic modulus of 104.8 GPa (15.2 Msi) were given by the manufacturer. For the GFRP bars these values were 724 MPa (105 ksi) and 41.4 GPa (6 Msi), respectively. A design compressive strength of 27.6 MPa (4000 psi) was used for the concrete in the FRP-RC bridge panels. Verification of the FRP and concrete material properties was conducted and is outlined in the "Laboratory Testing" section.

For the flexural design, the procedure is similar to that used in the case of steel reinforcement once the appropriate modes of failure are recognized. The two possible failure modes are (a) rupture of the FRP reinforcement prior to crushing of the concrete and (b) crushing of the concrete prior to rupture of the FRP reinforcement. According to ACI-440 (2) both modes of failure are acceptable; due to the linear-elastic behavior of FRP materials up to failure, the concrete crushing failure is marginally preferred because a small degree of plasticity is exhibited prior to failure. Compared to the flexural design strength reduction factor used in steel-reinforced concrete design (i.e., 0.9), the factors used for FRP-reinforced concrete range from 0.7, for concrete-controlled failure, to 0.5, for FRP-controlled failure, to account for the decreased ductility of the section. In this specific situation, the section was designed to ensure concrete crushing prior to rupture of the FRP bars.

For the shear design, the separate contributions to the shear capacity of the concrete,  $V_c$ , and the reinforcement,  $V_f$ , are still considered. However, the ratio  $\rho_f E_f / \rho_s E_s$  is used as a multiplier of the concrete shear strength contribution to account for the reduced stiffness of the FRP bars compared to steel reinforcing bars; the reduced stiffness will lead to larger shear cracks thereby decreasing the contribution of the concrete to the shear capacity. It should be noted that  $\rho_f$  is the reinforcement ratio of the FRP-RC section,  $E_f$  is the longitudinal modulus of elasticity of the FRP reinforcement,  $\rho_s$  is the reinforcement ratio of a steel-RC section of equal capacity, and  $E_s$  is the modulus of elasticity of the steel reinforcement. It should be underlined that the term "equal capacity" refers to the design flexural moment capacity,  $\phi M_n$ . The reinforcement ratio for the FRP-RC panels is 0.0116 and the corresponding steel reinforcement ratio for the same design moment capacity is 0.0121, yielding a value of 0.50 for the ratio of  $\rho_f E_f / \rho_s E_s$ .

Based on the material properties and design parameters, the longitudinal reinforcement consists of 12 bundles of three 9.5-mm (3/8-in) CFRP bars, while for the shear stirrups 9.5-mm (3/8-in) GFRP bars are utilized. Although their contribution to the flexural capacity of the member is not considered, 12.7-mm (1/2-in) GFRP bars are utilized in the top side of the cage. Transverse reinforcement consisting of 12.7-mm (1/2-in) GFRP bars at 1.2 m (4 ft) is also provided in the panels. Due to the fact that thermoset resins are used in the manufacturing of the FRP bars, the FRP manufacturer conducted all necessary bending of the reinforcing bars prior to their shipment to the concrete precaster. Figure 1a illustrates the layout of the FRP reinforcement in each panel. The flexural and shear capacities of the FRP-RC panels are discussed in detail in the "Laboratory Testing" section.

### Steel-RC Design

Design of the steel-RC panel was conducted in the traditional manner, according to ACI 318 guidelines, such that the ultimate capacity,  $M_n$ , of the panel was approximately equal to the ultimate moment capacity of the FRP-RC panel. The steel-RC panel was under-reinforced indicating that failure would be defined by yielding of the steel followed by crushing of the concrete. The reinforcement in the steel-reinforced panel consists of eight 22.2-mm (7/8-in) bars for the tensile longitudinal reinforcement, three 12.7-mm (1/2-in) bars for the compressive longitudinal reinforcement and 9.5-mm (3/8-in) bars for the shear reinforcement. Figure 1b illustrates the layout of the steel reinforcement in the panel. The design compressive strength of the concrete for the steel-RC panel was 27.6 MPa (4000 psi) and steel reinforcement with a yield strength of 413.7 MPa (60 ksi) was utilized; it should be underlined that a bi-linear constitutive model was assumed for the steel, neglecting any strain hardening that may occur. Verification of the steel and concrete material properties was conducted and is outlined in the "Laboratory Testing" section along with further discussion of the flexural and shear capacities of the steel-RC panel.

## FABRICATION AND INSTALLATION OF THE FRP-RC PANELS

The existing forms of the concrete precaster were utilized without modification. The FRP bars are considerable lighter than steel bars, which allows them to be moved by fewer workers. Due to the decreased stiffness, the bars deflect more and may require more support chairs during the assembly of the reinforcing cage. Plastic chairs were used to support the reinforcement cages within the forms during casting and plastic ties were used to secure the reinforcing bars in the desired reinforcement configuration. Note the plastic ties in Figure 1a.

Installation proceeded based on the following outline of tasks:

- Install precast concrete panels – place panels onto the abutments; connect panels; secure the panels to the abutments; fill the panel joints.
- Install the bridge guardrails – attach the guardrail posts to the panels; attach guardrail to posts.

Tasks unique to the use of precast concrete panels that warrant further attention are the connection of the panels to one another, the connection of the panels to the abutments, and the connection of the guardrail posts to the panels.

The connection of the panels together was accomplished through the use of steel angles, which were embedded in the panel edges and then welded together once the panels were in place on the abutments. This is the only steel detail left in the panels and work is currently in progress to develop a non-metallic means of connection. For the connection of the panels to the abutments, a void was formed approximately 0.15 m (6 in) from each end of each panel, through which a hole was drilled into the abutment to receive an anchor bolt. The anchor bolts were secured into the abutments with a two-part epoxy and a nut was tightened down to secure the panels. Once the panels were connected together and to the abutment, non-shrink grout was used to fill the joints and to cover the anchor bolts. The connection of the guardrails to the panels was accomplished using the same type of steel angles embedded at the panel joints. Once the guardrail posts were welded to the panels, the guardrails were bolted to the posts completing the installation of the bridge. The guardrails were designed to meet AASHTO design requirements.

Installation of the Walters Street Bridge began on June 18, 2001. Installation was completed and the bridge was officially opened to traffic on June 28, 2001. A cast-in-place concrete box culvert would have been the alternative to this bridge technology and would have taken significantly longer.

## **LABORATORY TESTING**

### **Material Characterization**

Characterization of the FRP bars was conducted in the laboratory to verify the tensile properties provided by the manufacturer. To avoid failure of the specimen at the grips due to the relatively low transverse strength of the FRP materials, the ends of the specimens were encased in steel pipe using an expansive grout. A gripping length of 38.1 cm (15 in) was used based on work conducted by Micelli et al. (3). Furthermore, an overall specimen length of  $40d_b$  plus two times the gripping length, where  $d_b$  is the diameter of the bar, was used based on provisional specifications for FRP bars testing that are under review by ACI committee 440. A comparison between the mean values obtained during laboratory testing (based on three specimens) and the manufacturer's recommended values is presented in Table 1.

Verification of the yield strength of the steel reinforcement was also conducted in the laboratory. The yield strength of the steel was reported at 414 MPa (60 ksi) by the manufacturer and the average strength determined from the three specimens tested was 416 MPa (60.4 ksi). Verification of the concrete strength was also conducted by coring cylinders from the tested RC panels. For the four concrete cylinders tested from each of the panels, the average compressive strength values were 27.3 MPa (3960 psi) and 22.5 MPa (3260 psi) for the steel-RC and FRP-RC panels, respectively.

### **Flexural Testing**

Testing of both specimens was conducted under four-point bending. The 7.32-m (24-ft) specimens were tested over a clear span of 6.4 m (21 ft) with the equal loads applied 2.74 m (9 ft) from each support, leaving a constant-moment region 0.91 m (3 ft) in length. Based on simple beam theory and a failure criterion of a maximum concrete strain of 0.003, the failure load was approximated at 210 kN (47 kips) for both the steel-RC and FRP-RC sections. The panels were tested to failure through the application of quasi-static load cycles. Several load cycles were conducted within each of the moment-curvature diagram regions (e.g., up to cracking, yielding of the steel, etc.). Each load cycle proceeded up to the desired load followed by unloading to approximately 22.24 kN (5 kips); during the final load cycle the specimen was taken to failure.

In addition to the linear variable differential transformer (LVDT) transducers, string transducers, and electrical resistance strain gages installed to the exterior of the specimens in the laboratory, electrical resistance strain gages were installed on the reinforcing bars prior to casting of the panels. Strain gages were located on several of the tension reinforcement and compression reinforcement bars at mid-span and on the shear stirrups at 0.51 m (20 in) and 0.76 m (30 in) from one end of the panel. The results of these

tests are summarized herein in terms of the moment-curvature diagrams, load-deflection diagrams and observed failure modes.

Figure 2 illustrates the moment-curvature relationships for the steel-RC and FRP-RC panels. For each panel the experimental envelope is plotted along with the theoretical relationship, which is tri-linear in the case of the steel-RC panel and bi-linear in the case of the FRP-RC panel. For the tri-linear moment-curvature relationship for the steel-RC panel, the cracking, yield and ultimate moment and curvature values were calculated. For the bi-linear moment-curvature relationship for the FRP-RC panel, the cracking and ultimate moment and curvature values were calculated. Both theoretical relationships were based on the following assumptions:

- Plane sections remain plain, that is, the concrete and reinforcement strain values are proportional to their distance from the neutral axis
- The tensile strength of the concrete is ignored.
- A parabolic stress distribution in the concrete was utilized.
- The ultimate concrete compressive strain is 0.003.
- There is perfect bond between the reinforcement and the concrete.

Specific to the reinforcement utilized, it was assumed that the FRP reinforcement exhibits linear-elastic behavior until failure and no strain hardening of the steel reinforcement was considered.

Failure of both panels was predicted at and occurred at approximately 298 kN-m (220 kip-ft). It should be noted that for the FRP-RC panel, the difference between the initial slope of the experimental curves and the initial slope of the theoretical curves is due to the presence of a crack near mid-span that had occurred during shipment. Very good agreement was observed between the theoretical and experimental stiffness values for both of the panels.

The load-deflection diagrams for the steel-RC and FRP-RC panels are illustrated in Figure 3. For the steel-RC section, the envelope of the experimental results is plotted against the theoretical load-deflection relationship, which is obtained via double-integration of the tri-linear approximation of the moment-curvature relationship. For the FRP-RC section, the envelope of the experimental results is plotted against the theoretical load-deflection relationship, which is obtained via double-integration of the bi-linear approximation of the moment-curvature relationship. Furthermore, the predicted load-deflection relationship for the FRP-RC panel as calculated utilizing the ACI-440 guidelines (2) is presented. Utilizing the modified Branson's equation presented by ACI, the effective moment of inertia of the section was determined for various levels of applied moment and used to calculate the deflection of the panel. The modified Branson's equation is as follows:

$$I_e = \left( \frac{M_{cr}}{M_a} \right)^3 \beta_d I_g + \left[ 1 - \left( \frac{M_{cr}}{M_a} \right)^3 \right] I_{cr} \leq I_g$$

where  $M_{cr}$  is the cracking moment of the section,  $M_a$  is the moment applied to the section,  $\beta_d$  is a modification factor based on the ratio of the modulus of the FRP reinforcement to that of steel reinforcement,  $I_g$  is the gross moment of inertia of the section and  $I_{cr}$  is the cracked moment of inertia of the section. As the ACI provisions intend to limit the deflections at service load levels, the ACI predicted load-deflection relationship is plotted up to the load that would induced the service moment in the panel.

Failure of the steel-RC panel occurred at a load of approximately 222.4 kN (50 kips) and was characterized by yielding of the tensile reinforcement followed by crushing of the concrete just outside the area of load application. Failure of the FRP-RC panel occurred at approximately 209.1 kN (47 kips), as indicated by shear cracking and crushing of the concrete. Failure of the steel-RC and FRP-RC panels during the flexural capacity tests is illustrated in Figures 4 and 5, respectively. The shear cracking of the FRP-RC panel in Figure 5 is highlighted with lines to make it more visible.

A comparison of the load-deflection curves of the FRP-RC and steel-RC panels confirms that the FRP-RC section is less stiff than the steel-RC section, however both sections reached the predicted failure load. For both sections, the slope of the experimental curve is nearly identical to the theoretical curve obtained from the moment-curvature relationship, however the ACI-440 theoretical curve exhibits a much lower stiffness than the other two curves for the FRP-RC section. A comparison of the ACI-440 theoretical deflection, a value of approximately 103.4 mm (4.1 in) at the service load level, and the experimental deflection, a value of approximately 52.9 mm (2.1 in) at the same load level, indicates that the experimental deflection is approximately 50 percent of the theoretical deflection as predicted by the ACI-440 guidelines (2). If the same comparison is drawn between the predicted deflection of the steel-RC panel based on the Branson equation and the experimental deflection, the ratio of experimental to theoretical deflection is also approximately 50 percent. The fact that the same level of conservatism is exhibited by both the Branson equation and the modified Branson equation lends confidence to the adoption of the modified Branson equation in the ACI-440 guidelines (2).

### Shear Testing

Following the flexural capacity testing, the same two panels were also tested to determine their shear capacity. The portion of the panels that were unaffected by the flexural testing were re-tested in three-point bending with a clear span of 2.13 m (7 ft). Instrumentation for the shear capacity tests consisted of string transducers and LVDT transducers. Furthermore, for the FRP-RC panel the strain gages located on the shear stirrups 0.51 m (20 in) and 0.76 m (30 in) from the end of the panel were connected to measure strain in the FRP stirrups at shear failure of the panel.

Utilizing the material properties obtained from the laboratory characterization and ACI guidelines for FRP and steel reinforced concrete, the ultimate shear capacity of the steel-RC and FRP-RC panels was predicted at approximately 314.5 kN (70.7 kips) and 137 kN (30.8 kips), respectively. The concrete contribution to the shear capacity is approximated by  $2\sqrt{f'_c}bd$  for the steel-RC and by

$\frac{\rho_f E_f}{\rho_s E_s} \left( 2\sqrt{f'_c}bd \right)$  for the FRP-RC. In the above relationships  $f'_c$  denotes the concrete compressive strength,  $b$  denotes the width of the panel, and  $d$  denotes the depth to the centroid of the reinforcing bars.

The reinforcement contribution to the shear capacity is approximated by  $\frac{A_v f_y d}{s}$  for the steel-RC and by

$\frac{A_{fv} f_{fv} d}{s}$  for the FRP-RC. In the above relationships  $A_v$  and  $A_{fv}$  denote the area of shear reinforcement for

the steel and FRP,  $f_y$  is the yield stress of the steel shear reinforcement,  $f_{fv}$  is the design stress level for the FRP shear reinforcement, and  $s$  denotes the spacing of the shear reinforcement. It should be underlined that the strain in the FRP shear reinforcement is limited to 0.002 by the ACI-440 guidelines (2). For the steel-RC panel, the concrete contribution to the shear strength is 193.9 kN (43.6 kips) and the reinforcement contribution is 120.4 kN (27.1 kips); for the FRP-RC section these values are 94.7 kN (21.3 kips) and 42.3 kN (9.5 kips), respectively.

Figure 6 illustrates the experimental load-deflection relationships obtained during the shear capacity testing. Failure of the steel-RC panel occurred at approximately 580 kN (130 kips). Failure of the FRP-RC panel occurred at approximately 525 kN (118 kips). The steel-RC and FRP-RC shear capacity predictions were very conservative, due in part to the factor of two assumed for the contribution of the concrete to the shear capacity, the ratio used to reduce the concrete contribution to the shear capacity of the FRP-RC panel, and the limit of 0.002 on the strain in the FRP shear reinforcement. Failure of the steel-RC and FRP-RC panels during the shear capacity tests is illustrated in Figures 7 and 8, respectively. In Figure 7, a line to make it more visible highlights the shear crack in the steel-RC section. The vertical dashed lines in Figure 8 represents the location of the instrumented stirrups located approximately 0.51 m (20 in) and 0.77m (30 in) from the end of the panel. Although it not visible in the figures, crushing of the concrete did occur at failure.

Strain readings from the shear stirrups are illustrated in Figure 9. Due to the test setup, the shear stirrups were located 50.8 mm (2 in) and 0.30 m (12 in) from the support, respectively. The two instrumented stirrups located 0.30-m (12-in) from the center of the support both experienced significant levels of strain. The stirrup in the right side of the panel exhibited more strain than that on the left side, however this is consistent with the shear cracking exhibited by the panel. This figure indicates the very conservative ACI-440 limit for the strain in the shear stirrups of 0.002 (marked on the figure by a dashed vertical line). The maximum strain experienced by the shear stirrups was roughly 0.0065, corresponding to roughly one-third the ultimate strain at rupture and a stress of approximately 250 MPa (36 ksi). Rupture of the FRP stirrups was not observed.

## FIELD TESTING

Instrumentation utilized during the testing included direct current variable transformer (DCVT) transducers, which were installed underneath the bridge to monitor deflection of the bridge panels. Six DCVT transducers were located at mid-span and six were located near the supports. Loading of the bridge was accomplished with a loaded tandem-axle dump truck placed at various locations on the bridge. The total weight of the truck was 212.98 kN (47,880 lb) with 66.19 kN (14,880 lb), 72.86 kN (16,380 lb), and 73.93 kN (16,620 lb), on each of the three axles from the front to the rear of the truck, respectively.

Several passes of the truck were made, each at a different transverse position on the bridge. This paper will examine the passes conducted at the center of the bridge (i.e., Pass 4); both static passes and passes at 32 kph (20 mph) were conducted at this location. During each pass the truck was stopped at five longitudinal locations. Due to the axle loads and axle spacing of the loading truck, truck location 3 corresponds to the worst-case loading condition. A more comprehensive discussion of the results of the load testing can be examined elsewhere.

The results of the load test for Pass 4 are presented in Figure 10. The illustration at the bottom of the figure depicts the layout of each of the nine panels and the lateral location of the tandem axles on the bridge. Furthermore, the dashed portion of the curve is mirrored from the actual measurements. The progression of the deflected shape from the top curve to the bottom curve is consistent with the level of moment induced by each loading position. Stop 1 generates the least moment in the bridge; followed by Stop 1; Stops 2 and 4, which are nearly identical; and Stop 3, which produces the largest bending moment.

The impact factor for the live load was examined by conducting a pass in the same location as Pass 4 at a speed of approximately 32 kph (20 mph) (see Figure 10). The impact factor was computed as the ratio of the deflection obtained at 32 kph (20 mph) to the deflection obtained at Stop 3. The six values, one for each DCVT, were averaged to obtain an impact factor of 0.25. Compared to the computed AASHTO impact factor for this bridge, which is 0.30, the AASHTO guidelines appear to be conservative.

Distribution of load between panels was also examined by comparing the deflection of the bridge panels to the theoretical load-deflection relationship based on the loading conditions during the load test. Utilizing the deflection obtained in the bridge load test, the load experienced by each panel individually was determined. A comparison of these loads quantifies the lateral distribution of load between the panels. It should be noted that the load-deflection relationship for an uncracked section was used. The use of the uncracked stiffness is justified because (a) the load induced during the load test in the panels, a maximum of approximately 12.0 kN (2.7 kips) is approximately 45 percent of the cracking load for the bridge panels and (b) it is unlikely that two fully-loaded trucks would be on the bridge at the same time given the surrounding community (i.e., the section should be uncracked).

The load distribution as a percent of the total load on the bridge was examined for all passes conducted. This analysis indicated a decrease in the maximum deflection as the load progressed toward the center of the bridge and illustrated that although the total load experienced by the bridge is greater in the case of the 32-kph (20-mph) pass due to impact, the percentage of load carried by each respective panel is very similar to that exhibited during the static Pass 4. Furthermore, the peak load percentage carried by Panel 4 is identical for the two passes. Further investigation into the distribution of load between panels,

via comparison of the distribution in the bridge to the distribution within a continuous slab, will allow the efficiency of the panels to be quantified.

The bridge panels themselves were designed to meet the AASHTO deflection requirement of span length divided by 800, which in this case corresponds to a deflection of 8.76 mm (0.345 in). The maximum observed deflection during the static load passes was 2.4 mm (0.094 in), yielding a span to deflection ratio of approximately 2940 or approximately one-quarter of the allowable deflections. Moreover, utilizing the principle of superposition and assuming linear-elastic behavior the predicted deflection of the bridge for the design loading condition of one truck in each of the two lanes was determined. The maximum deflection in this case is roughly 3.1 mm (0.12 in) for a span to deflection ratio of approximately 2300, or a deflection roughly one-third of the allowable deflection.

In an effort to monitor the long-term performance of the bridge in-situ, additional field load tests will be conducted annually for two more years. The deflection from year-to-year will be compared and any degradation will be quantified. The annual load test will also be combined with an inspection of the visible bridge components for possible wear and degradation.

## CONCLUSIONS

Based on the design, installation, and testing of FRP-RC and steel-RC panels conducted the following conclusions can be drawn:

- Utilizing FRP in the form of reinforcing bars allows for the use of many steel-RC concrete practices. The fabrication and installation details were nearly identical to the methods utilized by the concrete precaster for steel-reinforced panels.
- The experimental deflection of the FRP-RC panel in the laboratory was approximately 50 percent of the theoretical deflection as predicted by ACI-440 guidelines (2), which use the modified Branson equation, indicating that the ACI-440 flexural design guidelines are conservative.
- The same level of conservatism is exhibited by the ACI 318 guidelines, which use the Branson equation, lending credibility to the adoption of the modified Branson equation by ACI-440.
- Laboratory testing exhibited good agreement between the experimental and theoretical stiffness values based on moment-curvature predictions.
- The experimental shear capacity of the steel-RC and FRP-RC panels was approximately equal, with both panels exhibiting a considerably higher shear capacity than predicted.
- The limit of 0.002 on the strain in FRP shear reinforcement is partially responsible for the conservative predictions of the shear capacity for the FRP-RC panel by the ACI-440 guidelines (2).
- The deflection of the bridge panels during the in-situ bridge load test appears to be reasonable with a maximum deflection of approximately 2.5 mm (0.1 in) occurring during the 32-kph (20-mph) pass.
- A span-to-deflection ratio of 2300 (or approximately one-third of the maximum allowable deflection) was predicted for the design loading condition of one truck in each of the two lanes of the bridge.
- The load impact factor for the bridge was quantified as 0.25.

## ACKNOWLEDGEMENTS

The authors would like to acknowledge funding and support received from the University Transportation Center at the University of Missouri – Rolla, the Missouri Department of Transportation, the City of St. James, the National Science Foundation, and the Missouri Department of Economic Development. Thanks is extended to Marshall Industries Composites, Inc., the manufacturer of the FRP bars utilized in this project, and Oden Enterprises, Inc., who was responsible for the precasting of the bridge panels and the installation of the bridge.

## REFERENCES

1. Stone, D., A. Nanni, and J. Myers. Field and Laboratory Performance of FRP Bridge Panels. In *Proceedings of the International Conference on Composites in Construction - CCC 2001*, Porto, Portugal, Oct. 10-12, 2001.
2. ACI Committee 440. *Guide for the Design and Construction of Concrete Reinforced with FRP Bars*. 440.1R-01, American Concrete Institute, Farmington Hills, MI, 2001, pp. 41.
3. Micelli, F. and A. Nanni. *Mechanical Properties and Durability of FRP Rods*. CIES report 00-22, March 2001.

## **LIST OF TABLES AND FIGURES**

FIGURE 1 FRP and steel reinforcement layouts.

TABLE 1 Comparison of laboratory results and manufacturer's recommended values

FIGURE 2 Experimental and theoretical load-deflection relationships for the steel-RC and FRP-RC panels.

FIGURE 3 Experimental and theoretical moment-curvature relationships for the steel-RC and FRP-RC panels.

FIGURE 4 Failure of the steel-RC panel during the flexural testing.

FIGURE 5 Failure of the FRP-RC panel during the flexural testing.

FIGURE 6 Experimental load-deflection relationships for the shear testing of the steel-RC and FRP-RC panels.

FIGURE 7 Shear failure of the steel-RC panel.

FIGURE 8 Shear failure of the FRP-RC panel.

FIGURE 9 Strain in stirrups located at 0.3 m (12 in) from the support during the shear capacity test of the FRP-RC panel.

FIGURE 10 Deflected shape of the bridge for Pass 4.



**FIGURE 1 FRP and steel reinforcement layouts.**

**TABLE 1 Comparison of laboratory results and manufacturer's recommended values**

	Failure Stress			Modulus of Elasticity		
	Manufacturer Data (MPa)	Laboratory Data (MPa) [Standard Deviation]	Difference (%)	Manufacturer Data (GPa)	Laboratory Data (GPa) [Standard Deviation]	Difference (%)
<b>CFRP 9.5 mm</b>	1862	2155 [39.6]	+15.7	104.8	114.6 [7.6]	+9.2
<b>GFRP 9.5 mm</b>	779.1	873 [22.6]	+12.0	41.4	37.2 [3.3]	-10.0
<b>GFRP 12.7 mm</b>	723	798 [0]	+10.4	41.4	36.1 [0.7]	-12.5

Conversion factors: 1 in. = 25.4 mm, 1 psi = 6.89 kPa

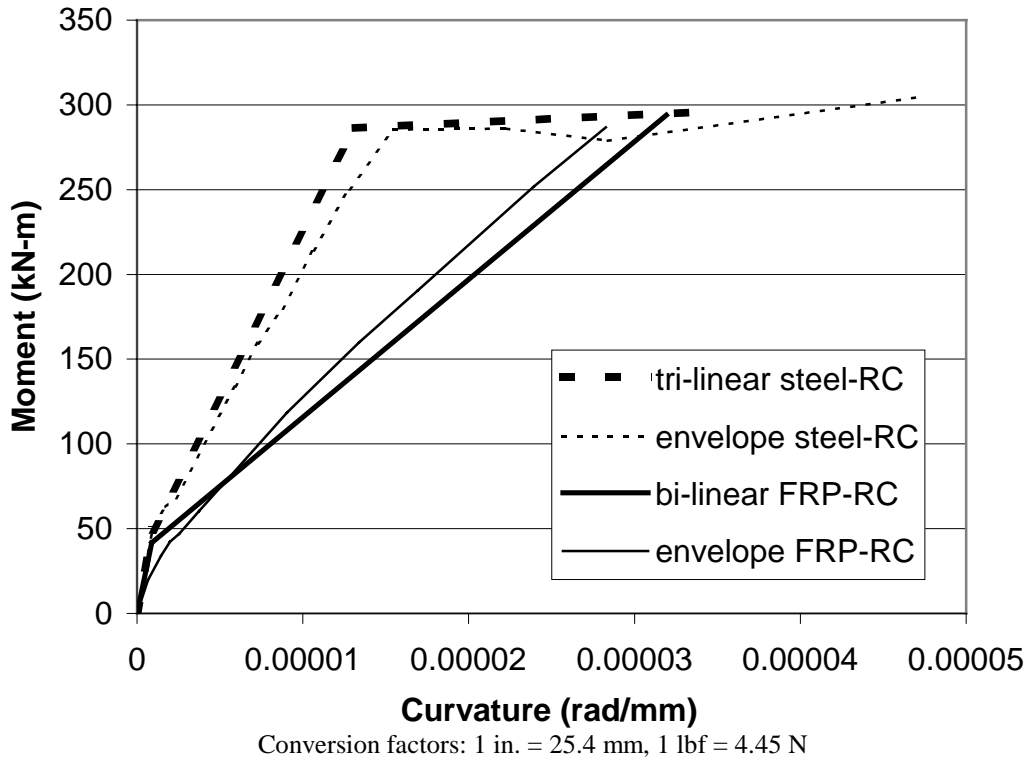


FIGURE 2 Experimental and theoretical moment-curvature relationships for the steel-RC and FRP-RC panels.

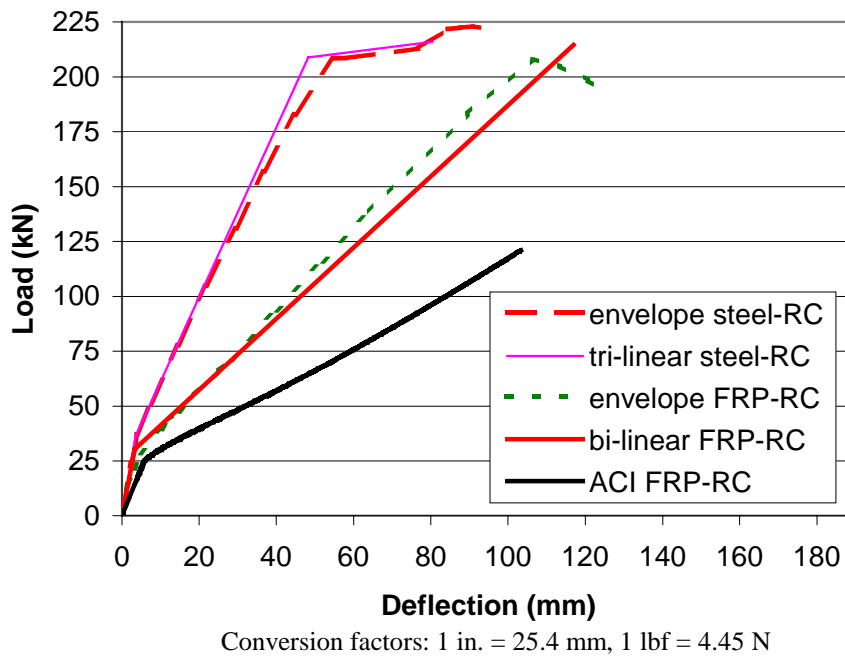


FIGURE 3 Experimental and theoretical load-deflection relationships for the steel-RC and FRP-RC panels.



FIGURE 4 Failure of the steel-RC panel during the flexural testing.



FIGURE 5 Failure of the FRP-RC panel during the flexural testing.

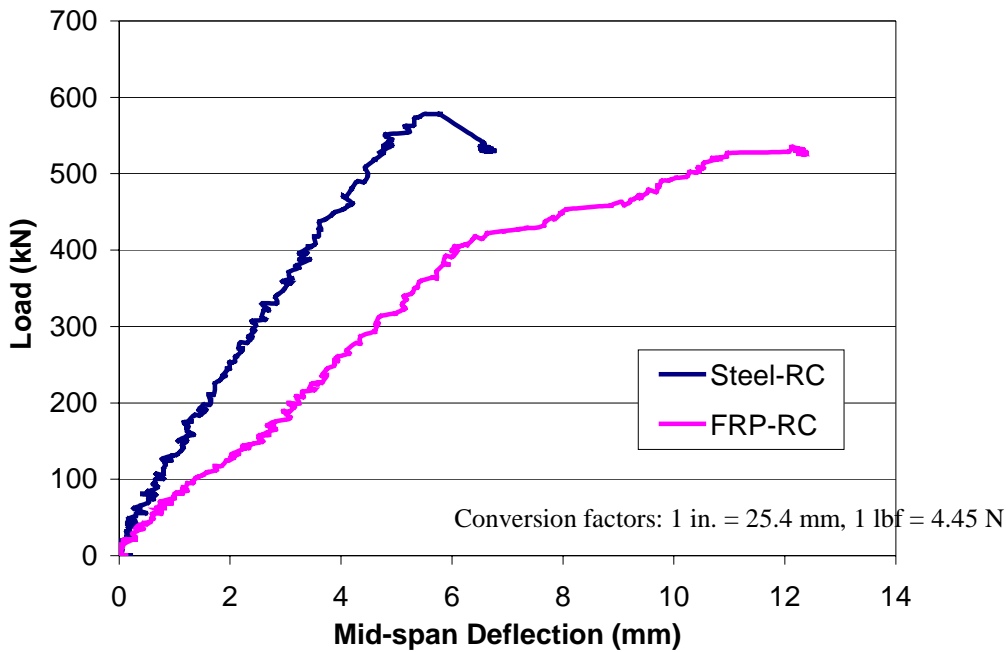
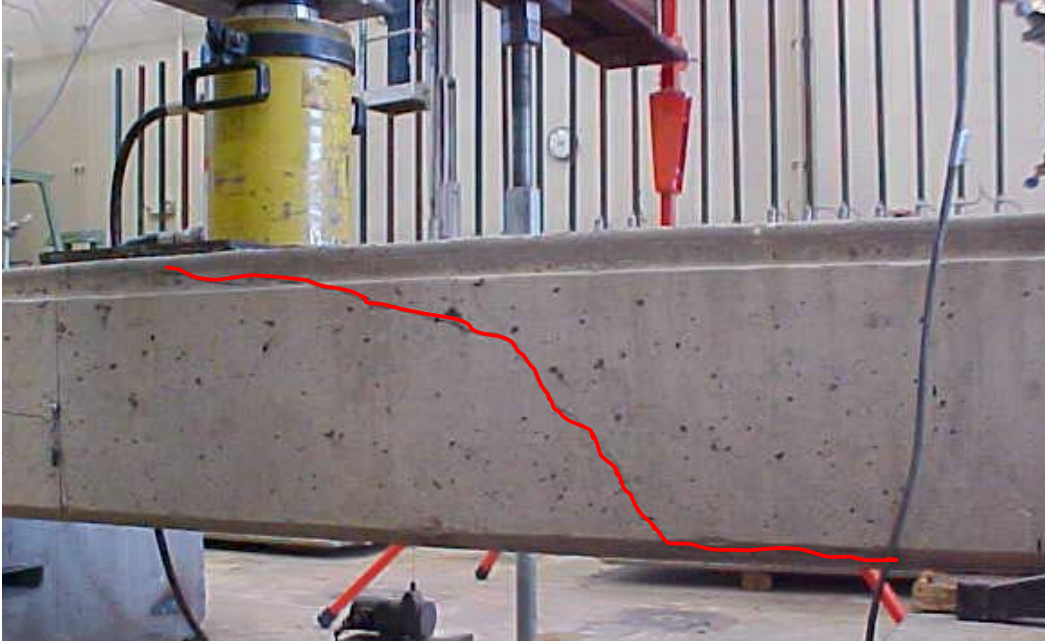


FIGURE 6 Experimental load-deflection relationships for the shear testing of the steel-RC and FRP-RC panels.



**FIGURE 7** Shear failure of the steel-RC panel.



**FIGURE 8** Shear failure of the FRP-RC panel.

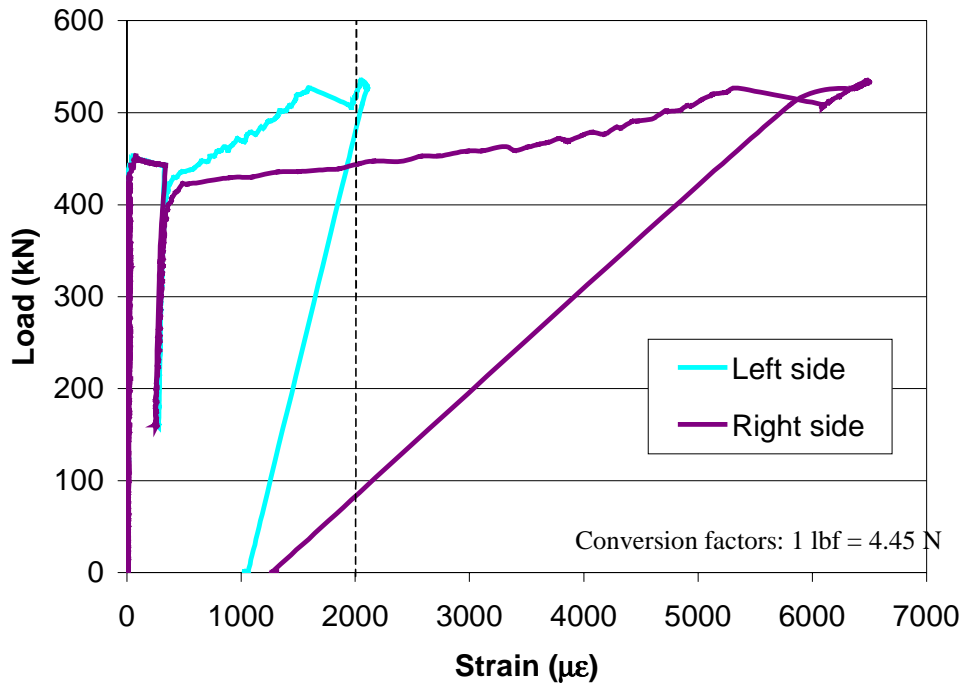


FIGURE 9 Strain in stirrups located at 0.3 m (12 in) from the support during the shear capacity test of the FRP-RC panel.

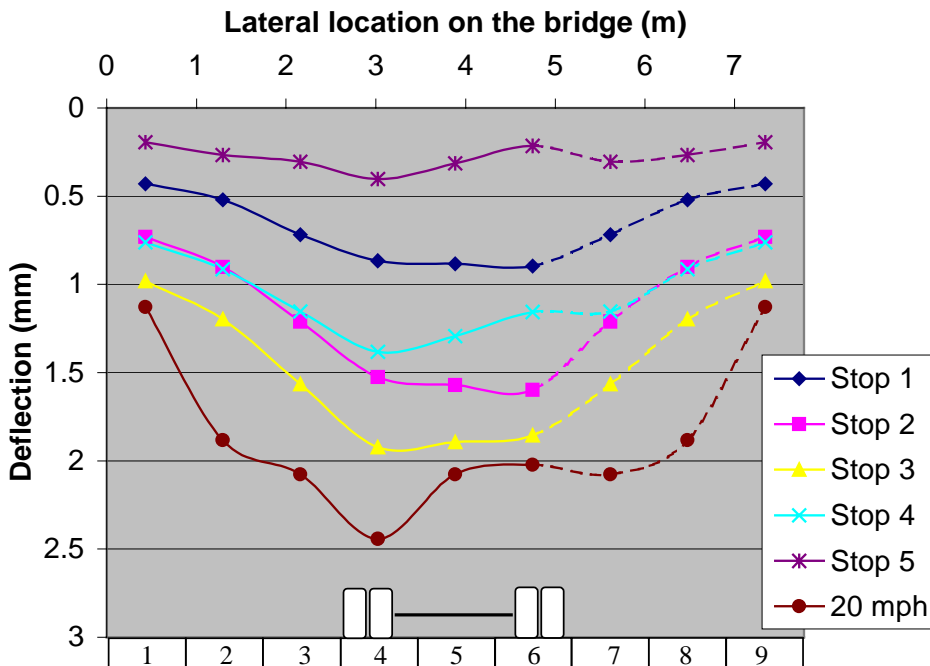


FIGURE 10 Deflected shape of the bridge for Pass 4.